European Journal of Radiology 176 (2024) 111538

Contents lists available at ScienceDirect

European Journal of Radiology

journal homepage: www.elsevier.com/locate/ejrad

Research article

Novel motion correction algorithm improves diagnostic performance of CT fractional flow reserve

Wenli Yang [a,1], Lihua Yu [a,1], Yarong Yu [a], Xu Dai [a], Wenyi Yang [b], Jiayin Zhang [a,*]

[a] Department of Radiology, Shanghai General Hospital, Shanghai Jiao Tong University School of Medicine, #85 Wujin Rd, Shanghai, China
[b] Department of Cardiology, Shanghai General Hospital, Shanghai Jiao Tong University School of Medicine, #85 Wujin Rd, Shanghai, China

ARTICLE INFO

Keywords:
Coronary artery disease
Coronary computed tomographic angiography
Fractional flow reserve
Motion correction

ABSTRACT

Objectives: This study aimed to investigate the diagnostic performance of computed tomography (CT) fractional flow reserve (CT-FFR) derived from standard images (STD) and images processed via first-generation (SnapShot Freeze, SSF1) and second-generation (SnapShot Freeze 2, SSF2) motion correction algorithms.

Methods: 151 patients who underwent coronary CT angiography (CCTA) and invasive coronary angiography (ICA)/FFR within 3 months were retrospectively included. CCTA images were reconstructed using an iterative reconstruction technique and then further processed through SSF1 and SSF2 algorithms. All images were divided into three groups: STD, SSF1, and SSF2. Obstructive stenosis was defined as a diameter stenosis of ≥ 50 % in the left main artery or ≥ 70 % in other epicardial vessels. Stenosis with an FFR of ≤ 0.8 or a diameter stenosis of ≥ 90 % (as revealed via ICA) was considered ischemic. In patients with multiple lesions, the lesion with lowest CT-FFR was used for patient-level analysis.

Results: The overall quality score in SSF2 group (median = 3.67) was markedly higher than that in STD (median = 3) and SSF1 (median = 3) groups ($P < 0.001$). The best correlation ($r = 0.652$, $P < 0.001$) and consistency (mean difference = 0.04) between the CT-FFR and FFR values were observed in the SSF2 group. At the per-lesion level, CT-FFR$_{SSF2}$ outperformed CT-FFR$_{SSF1}$ in diagnosing ischemic lesions (area under the curve = 0.887 vs. 0.795, $P < 0.001$). At the per-patient level, the SSF2 group also demonstrated the highest diagnostic performance.

Conclusion: The SSF2 algorithm significantly improved CCTA image quality and enhanced its diagnostic performance for evaluating stenosis severity and CT-FFR calculations.

1. Introduction

As the first-line test in patients with coronary artery disease (CAD), coronary computed tomography angiography (CCTA) has shown favorable diagnostic performance in identifying and excluding anatomical obstructive coronary artery stenosis [1,2]. However, the correlation between anatomic CAD stenosis and myocardial ischemia remains poor. Traditional CCTA anatomical parameters lack the ability to evaluate the hemodynamic significance of lesions, potentially leading to unnecessary invasive coronary angiography (ICA) [3–5].

Coronary computed tomography-derived fractional flow reserve (CT-FFR) is a noninvasive imaging modality that uses CCTA-derived coronary artery tree data and fluid dynamics modeling to simulate pressure decay before and after stenosis [6]. This technique can accurately identify ischemic and nonischemic lesions and has exhibited high consistency with invasive FFR calculations in previous studies [7,8]. However, the diagnostic performance of CT-FFR depends on an accurate segmentation of the coronary artery lumen. Motion artifacts in CCTA images can substantially impair the segmentation quality, leading to a decline in the diagnostic accuracy of CT-FFR [9]. Thus, minimizing

Abbreviations: AUC, area under the curve; CACS, Coronary artery calcium score; CAD, coronary artery disease; CT-FFR, coronary computed tomography-derived fractional flow reserve; CTO, Chronic total occlusion; DS, diameter stenosis; FFR, Fractional flow reserve; ICA, invasive coronary angiography; LM, left main artery; NPV, negative predictive value; PPV, positive predictive value; ROC, receiver operating characteristic; SSF1, SnapShot Freeze; SSF2, SnapShot Freeze 2; STD, standard.

* Corresponding author.
E-mail address: andrewssmu@msn.com (J. Zhang).

[1] Dr. Wenli Yang and Dr. Lihua Yu contributed equally to this study.

https://doi.org/10.1016/j.ejrad.2024.111538
Received 19 January 2024; Received in revised form 23 April 2024; Accepted 28 May 2024
Available online 29 May 2024

motion artifacts in CCTA and enhancing image quality to ensure the reliability and effectiveness of CT-FFR in routine clinical practice are vital.

The first-generation motion correction algorithm (SnapShot Freeze, SSF1; GE Healthcare), introduced in 2012, is a coronary artery motion artifact correction algorithm [10]. SSF1 utilizes data from three adjacent phases of the same cardiac cycle, centering on the middle phase, to track and compensate for coronary artery motion, effectively reducing motion artifacts. Accurately characterizing the path and velocity of vessel motion determines the position of the coronary vessels at the target phase, adaptively compensating for any residual motion. Its application significantly improves the image quality of coronary arteries in patients with high heart rates[11,12]. However, SSF1 fails to address structures other than the coronary arteries, resulting in uncorrectable cardiac motion artifacts in some patients. This limitation may lead to inaccuracies in CCTA for evaluating stenosis severity and CT-FFR calculation. Building upon the foundation of its predecessor, the second-generation whole-heart motion correction algorithm SnapShot Freeze 2 (SSF2, GE Healthcare) extended the correction range to the entire heart, further reducing motion artifacts of the coronary vasculature and myocardium [13]. The improvement of this technology may play a significant role in enhancing CCTA image quality and CT-FFR calculation accuracy.

Therefore, we hypothesized that SSF2, by improving coronary motion correction and lumen segmentation accuracy, can enhance the diagnostic accuracy of CT-FFR. This study aimed to explore the diagnostic efficacy of CT-FFR simulations using standard (STD), SSF1-corrected, and SSF2-corrected CCTA images, with invasive examination results as the reference standard.

2. Methods

2.1. Patient population

In this retrospective study, patients with intermediate-to-high pretest probability of CAD or patients with known CAD, who underwent both CCTA and ICA/invasive FFR examination within 3 months, were screened from January 2020 to May 2023. The exclusion criteria comprised patients with a history of myocardial infarction or target vessel revascularization. Institutional review board approval was obtained for this retrospective study, and obtaining informed consent from all patients was exempted.

2.2. CT acquisition protocol

All CCTA examinations were conducted using a 256-row wide detector CT scanner (Revolution HD, GE Healthcare, USA). Oral β-blocker (25–50 mg, Betaloc ZOK, AstraZeneca, China) was administrated 1 h before examination in patients with a heart rate of $>$ 80 bpm. Nitroglycerin tablets (0.5 mg, manufactured by Jingyi, Beijing Yimin Pharmaceuticals) were administered sublingually to all patients before scan. Coronary artery calcium score (CACS) scan was performed to evaluate the calcium burden of the epicardial artery. CCTA was performed after injection of 50–70 mL of the contrast agent iomeprol (Iomeron, 400 mg iodine/mL, Bracco, China) at 4–5 mL/s. A prospective electrocardiogram-triggered CCTA, covering 30 %–80 % of the R–R interval, was performed for scan acquisition. Automated tube voltage and current modulation (KV Assist, Smart mA, GE Healthcare, USA) were employed. The scanning parameters included a 280-ms rotation time, 256 $\times$ 0.625-mm collimation, 0.625-mm reconstruction section thickness, and 0.5-mm reconstruction section interval.

2.3. CCTA image analysis

The cardiac phases with the least number of motion artifacts were selected for image reconstruction. All images were reconstructed using the standard (STD, without motion correction) algorithm with 40 % adaptive statistical iterative reconstruction-v (ASIR-V, GE Healthcare) to decrease image noise. On this basis, motion correction was performed using the SSF1 and SSF2 algorithms (based on images from 60 ms before and after the target phase), respectively. Three datasets (STD, SSF1, and SSF2) were transferred to an offline workstation (ADW 4.7, GE Healthcare) for further analysis using standard formats (axial, cross-sectional, multiplanar reformation, curved multiplanar reformation, and three-dimensional maximum intensity projection).

The quality of the CCTA images was assessed using the Likert scale by two experienced radiologists (with 12 and 3 years of experience in cardiac CT imaging, respectively): a score of 4 indicates excellent image quality with no motion artifacts; a score of 3 indicates mild artifacts with good image quality, but fully evaluable and diagnostic; a score of 2 indicates moderate artifacts but acceptable for routine clinical diagnosis; and a score of 1 indicates severe artifacts with most of the vascular contours rendered unclear and nondiagnostic [14].

All coronary artery segments with a diameter of $\geq$ 1.5 mm were assessed. Diameter stenosis (DS) was defined as (reference diameter – minimal lumen diameter) / reference diameter. The mean DS value of measurements taken by the two radiologists was recorded for further analysis. Any disagreement between them was resolved by consensus.

2.4. CT-FFR calculation

CT-FFR simulation was performed using a dedicated software (CtaPlus; version 2.0, Pulse Medical Imaging Technology, China) based on quantitative flow ratio (QFR) technology [15]. Good diagnostic concordance between this technology and invasive FFR was observed in previous studies [16,17].

First, the software automatically analyzed all coronary artery segments, and all coronary arteries were merged into a hierarchical tree structure. Second, the reference lumen (the normal lumen without stenosis) was reconstructed, and the vessel centerline and luminal contours were manually adjusted as necessary. Finally, the QFR algorithm was used to calculate the CT-FFR values at each position of the reconstructed coronary tree. Lesion-specific CT-FFR values were measured 1–2 cm distal to the lesion for coronary stenosis on major epicardial vessels with a diameter of $\geq$ 1.5 mm [18]. Lesions with a CT-FFR value of $\leq$ 0.80 were defined as ischemic lesions. If multiple stenosis was noted, the CT-FFR value distal to the most severe lesion was used for patient-level analysis.

The two aforementioned radiologists independently analyzed CT-FFR without knowledge of the clinical history and invasive examination results. The average CT-FFR values measured by the two radiologists were used for further analysis.

2.5. ICA and invasive FFR measurements

The ICA examination was performed following standard procedures. Angiographic views from at least two orthogonal projections were obtained to diagnose the degree of stenosis. Invasive FFR was selectively measured in lesions with 30 %–90 % stenosis. Intravenous infusion of adenosine triphosphate (160 μg/kg/min) was administered to achieve maximal hyperemia, and FFR measurements were taken thereafter. All ICA procedures were evaluated by two interventional cardiologists with over 10 years of experience.

Ischemic lesions were defined as stenosis with an invasive FFR of $\leq$ 0.8 or DS of $\geq$ 90 %, whereas nonischemic lesions were defined as those with an FFR of $>$ 0.8 [19]. Chronic occlusion was excluded from the analysis. The observed outcome was the presence of ischemic lesions in the coronary arteries.

2.6. Statistical analysis

Statistical analyses were performed using SPSS version 26.0 and R version 4.2.1. Continuous variables with normal distribution were reported as mean ± standard deviation, whereas skewed variables were presented as median with interquartile range (Q1–Q3). Between-group differences were compared using the Mann–Whitney *U* test. The correlation between CT-FFR and FFR was assessed using Spearman's correlation coefficient. Consistency between CT-FFR and FFR was assessed using the Bland–Altman plot. The diagnostic performance of CCTA for assessing stenosis severity and CT-FFR from the three groups was compared using receiver operating characteristic curves. The area under the curve (AUC) was compared using the DeLong test. The accuracy, sensitivity, specificity, positive predictive value (PPV), and negative predictive value (NPV) were recorded, and the McNemar's test was used to obtain the P values between groups. A two-sided P-value of < 0.05 was considered statistically significant. The endpoint was the diagnostic performance of CT-FFR derived from different image datasets. A power value > 0.80 indicates there is sufficient sample size and sensitivity to detect significant differences in AUC values between groups at a significance level of 0.05.

3. Results

3.1. Patient characteristics

A total of 194 patients were retrospectively screened for inclusion. Thirty-one patients with a history of myocardial infarction or target vessels with a history of coronary revascularization were initially excluded before inclusion. Twelve patients with poor quality CCTA images based on STD, SSF1, and SSF2 were further excluded. Finally, 151 patients (170 lesions, mean age = 65.15 ± 8.93 years, 111 men) were enrolled (Fig. 1). There were 84 ischemic lesions, of which 31 showed an FFR of ≤ 0.8 and 53 showed DS of ≥ 90 %. The median radiation dose of CCTA was 2.80 mSv, and the average CT contrast medium usage was 46.94 ± 3.90 m. Table 1 presents the detailed demographic data.

Online supplement Table S1 indicated good interobserver consistency for all parameters, with ICC values exceeding 0.85. Compared with the STD and SSF1 groups, the SSF2 group had the highest overall image quality score with a median of 3.67 (Table 2). In different vessels, the image quality scores of the SSF2 group for the left anterior descending artery (LAD), left circumflex artery (LCx), and right coronary artery (RCA) were significantly higher than those of the SSF1 and STD groups (P < 0.001). However, no significant difference was found for the image quality between LAD and LCx in the STD and SSF1 groups (P > 0.05).

Table 1
Patient characteristics.

Patient characteristics (n = 151)	
Age, years	65.15 ± 8.93
Male, n (%)	111 (73.3)
BMI, kg/m^2	24.22 (22.69–26.29)
Hypertension, n (%)	103 (68.7)
Diabetes,n (%)	72 (48.0)
Dyslipidemia, n (%)	20 (13.3)
Current smoker, n (%)	31 (20.7)
Known CAD, n (%)	9 (6.0)
Pre-test probability of CAD*	
15 %-65 %, n (%)	12 (8.5)
65 %-85 %, n (%)	79 (55.6)
>85 %, n (%)	51 (35.9)
Prior percutaneous coronary intervention(non-target vessels), n (%)	9 (6.0)
CACS	243.5 (53.35–610.02)
0, n (%)	9 (6.3)
0–100, n (%)	44 (31.0)
100–400, n (%)	39 (27.5)
≥400, n (%)	50 (35.2)
CT effective radiation dose, mSv	2.80 (2.22–3.84)
Heart rate during CCTA, beats/min	64 (61–73)
CT contrast medium usage, mL	45.0 (40.0–50.0)
ICA contrast medium usage, mL	50.5 (50.0–60.0)

Abbreviations: CACS = coronary artery calcium score; CAD = coronary artery disease; CCTA = coronary computed tomography angiography; ICA = invasive coronary angiography.
Values are mean ± standard deviation, n (%), or median (IQR).
* Calculated based on the updated Diamond-Forrester model.

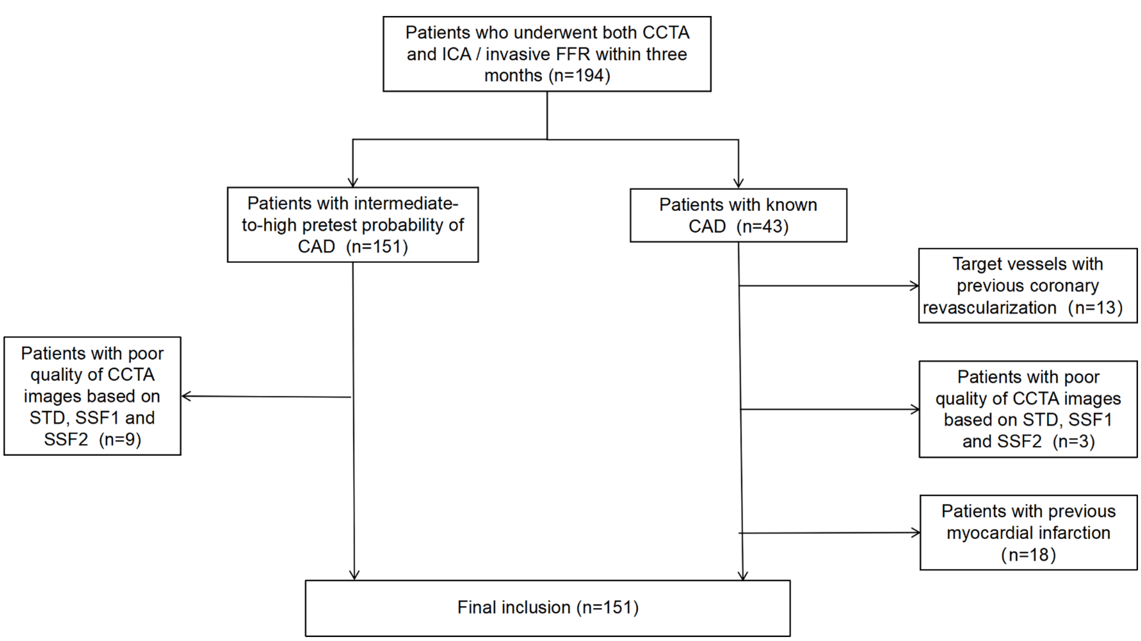

Fig. 1. Inclusion and exclusion flowchart. Abbreviations: CAD = coronary artery disease; CCTA = coronary computed tomography angiography; FFR = fractional flow reserve; ICA = invasive coronary angiography; SSF1 = SnapShot Freeze; SSF2 = SnapShot Freeze 2; STD = standard Pre-test probability of CAD was calculated based on the updated Diamond-Forrester model.

Table 2
Comparison of image quality scores in CCTA based on standard reconstruction and two motion correction algorithms.

Image quality score	STD	SSF1	P (STD vs SSF1)	SSF2	P (STD vs SSF2)	P (SSF1 vs SSF2)
LAD	3 (3 – 4)	3 (3 – 4)	0.058	4 (4 – 4)	<0.001	<0.001
LCx	3 (3 – 4)	3 (3 – 4)	0.076	3 (3 – 4)	<0.001	<0.001
RCA	3 (3 – 4)	3 (3 – 4)	0.001	4 (4 – 4)	<0.001	<0.001
Overall	3 (2.33 – 3.33)	3 (3 – 4)	0.007	3.67 (3.67 – 4)	<0.001	<0.001

Abbreviations: LAD = left anterior descending; LCx = left circumflex; RCA = right coronary angiography; SSF1 = SnapShot Freeze 1; SSF2 = SnapShot Freeze 2; STD = standard.
Values are median (IQR).

3.2. Comparison of DS evaluated by CCTA based on standard reconstruction and motion correction algorithms

Table 3 summarizes the diagnostic performance of DS evaluated using CCTA in detecting obstructive stenosis. The analysis at per-vessel level was presented in Online Supplementary Table S2. At both per-lesion (AUC = 0.898) and per-patient (AUC = 0.901) levels, the diagnostic performance of the SSF2 group was significantly higher than that of the STD and SSF1 groups (Figs. 2 and 3). At the per-patient level, compared with the SSF1 group, the SSF2 group demonstrated a 50 % increase in specificity (71.05 % vs. 47.37 %). It is noteworthy that irrespective of motion correction, DS evaluated using CCTA (defined as LM ≥ 50 % or other epicardial vessels ≥ 70 %) failed to accurately evaluate the hemodynamic significance of lesions. At both the per-lesion and per-patient levels, despite demonstrating high sensitivity and NPV, DS evaluated using CCTA in the SSF2 group showed both specificity and PPV of < 50 % in detecting ischemic lesions (Table 4).

3.3. Comparison of CT-FFR based on standard reconstruction and the two motion correction algorithms

The correlation and consistency between CT-FFR and FFR are presented in Fig. 4. At the per-lesion level, the SSF2 group exhibited the highest correlation between CT-FFR and FFR ($r = 0.652$, $P < 0.001$). There was good consistency of per-lesion CT-FFR values with FFR values, with a slight underestimation of CT-FFR values compared with measured FFR values. The SSF2 group showed a mean difference of 0.04 (95 % confidence interval [CI]: −0.13–0.20), with only 4.3 % (5/117) falling outside the 95 % CI, demonstrating the best consistency among the three groups.

At the per-lesion level, in the diagnosis of ischemic lesions, the diagnostic performance of CT-FFR in the SSF2 group was significantly better than that of the SSF1 group (AUC = 0.930 vs. 0.847, $P < 0.001$), with a post-hoc power analysis showing a power of 0.99, exceeding 0.80. The SSF2 group also exhibited the highest sensitivity and NPVs among the three groups, reaching 90.48 % and 89.87 %, respectively. Additionally, at the per-patient level and per-vessel level, the SSF2 group showed the highest diagnostic performance (Online Supplementary Table S3, Table 4 and Fig. 5).

Furthermore, compared with CCTA, CT-FFR revealed higher specificity and PPV in detecting ischemic stenosis. In patients with calcium scores of ≥ 400 and < 400, the SSF2 group demonstrated the highest diagnostic value for CT-FFR, with accuracy of 84.00 % and 84.78 %, respectively (Online supplement Table S4).

4. Discussion

This study highlighted the superiority of SSF2 over SSF1 in improving CCTA image quality. Additionally, DS assessment and CT-FFR simulation based on SSF2-corrected images exhibited the highest diagnostic accuracy in identifying obstructive stenosis and ischemic lesions.

Compared with traditional CCTA, CT-FFR has higher specificity and PPV in detecting hemodynamically significant coronary artery stenosis [6]. It is valuable in evaluating myocardial ischemia, guiding treatment strategies, and providing prognostic information [20]. However, CT-FFR calculation is substantially influenced by CCTA image quality. High heart rates and arrhythmias can induce motion artifacts during routine CCTA examinations. Xu et al. reported that the CCTA image quality score is a key factor influencing CT-FFR calculations, with the highest diagnostic accuracy observed when using CCTA images with a quality score of 4 [21]. In clinical practice, CT-FFR simulation may exhibit decreased accuracy due to the presence of cardiac motion artifacts in CCTA images. Our study aimed to reduce CCTA motion artifacts and

Table 3
Diagnostic performance of CCTA for identifying obstructive stenosis based on standard reconstruction and two motion correction algorithms.

Level	Group	Accuracy%	Sensitivity%	Specificity%	PPV%	NPV%
Per-lesion (n = 170)	STD	80.00 (136 / 170)	97.54 (119 / 122)	35.42 (17 / 48)	79.33 (119 / 150)	85.00 (17 / 20)
	SSF1	84.12 (143 / 170)	97.54 (119 / 122)	50.00 (24 / 48)	83.21 (119 / 143)	88.89 (24 / 27)
	P_1	<0.001	0.577	<0.001	0.624	<0.001
	SSF2	91.18 (155 / 170)	98.36 (120 / 122)	72.92 (35 / 48)	90.23 (120 / 133)	94.59 (35 / 37)
	P_2	<0.001	0.644	<0.001	0.683	<0.001
	P_3	<0.001	0.644	<0.001	0.676	<0.001
Per-patient (n = 151)	STD	81.46 (123 / 151)	98.23 (111 / 113)	31.58 (12 / 38)	81.02 (111 / 137)	85.71 (12 / 14)
	SSF1	85.43 (129 / 151)	98.23 (111 / 113)	47.37 (18 / 38)	84.73 (111 / 131)	90.00 (18 / 20)
	P_1	<0.001	0.702	0.004	0.733	<0.001
	SSF2	91.39 (138 / 151)	98.23 111 / 113	71.05 (27 / 38)	90.98 (111 / 122)	93.10 (27 / 29)
	P_2	<0.001	0.702	<0.001	0.733	<0.001
	P_3	<0.001	0.702	<0.001	0.727	<0.001

Abbreviations: NPV = negative predictive value; PPV = positive predictive value; SSF1 = SnapShot Freeze 1; SSF2 = SnapShot Freeze 2; STD = standard.
* Obstructive stenosis was defined as DS of left main artery (LM) ≥ 50 % or other epicardial vessels ≥ 70 %.
P_1:p-value for the comparison between the STD group and the SSF1 group.
P_2:p-value for the comparison between the STD group and the SSF2 group.
P_3:p-value for the comparison between the SSF1 group and the SSF2 group.

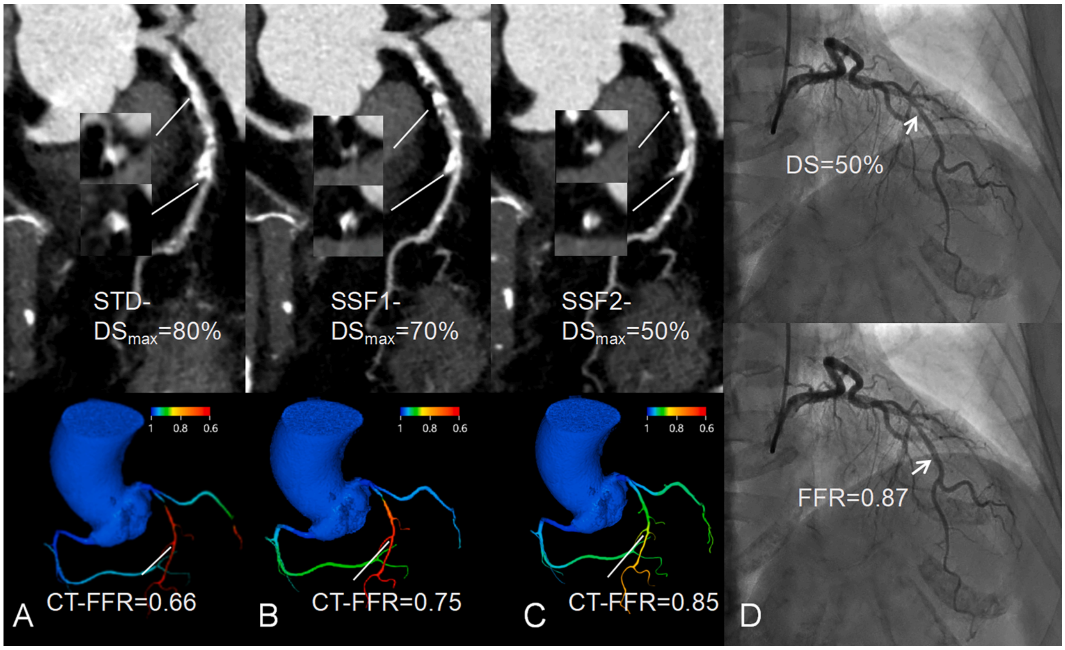

Fig. 2. Representative example of a 63-year-old man with stable angina. (A) Coronary computed tomography angiography (CCTA) images based on standard reconstruction showing significant artifacts in the proximal left anterior descending artery (LAD), with an image quality score of 2. The diameter stenosis (DS) of the most severe lesion was approximately 80 % and the CT-FFR result was 0.66, indicating an ischemic lesion. (B) CCTA images further processed with SSF1 also demonstrated artifacts in the proximal LAD, with an image quality score of 3. The DS of the most severe lesion was approximately 70 %, and the CT-FFR result was 0.75. (C) The CCTA images based on SSF2 demonstrated a significant improvement in the image quality of the proximal LAD, with an image quality score of 4. The measured diameter stenosis was approximately 50 %. The CT-FFR result in group SSF2 was 0.85, indicating a nonischemic lesion, which was consistent with the ICA and FFR results. (D) ICA and FFR results. Abbreviations: CCTA = coronary computed tomography angiography; CT-FFR = coronary computed tomography-derived fractional flow reserve; DS = diameter stenosis; FFR = fractional flow reserve; ICA = invasive coronary angiography; LAD = left anterior descending; SSF1 = SnapShot Freeze; SSF2 = SnapShot Freeze 2; STD = standard.

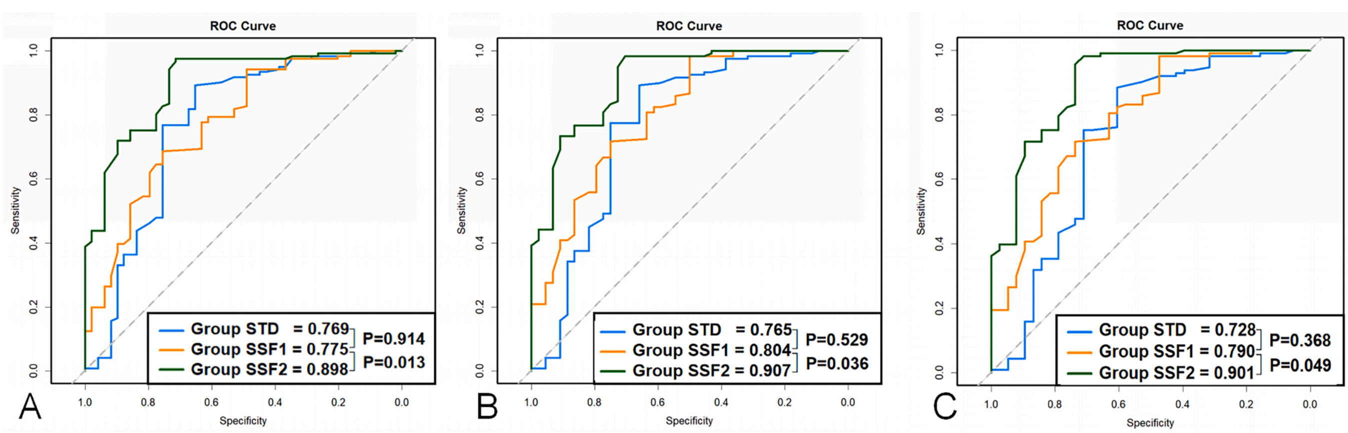

Fig. 3. ROC curves of the diameter stenosis evaluated by CCTA for the demonstration of obstructive stenosis at the per-lesion (A), per-vessel level (B) and per-patient level (C). Abbreviations: CCTA = coronary computed tomography angiography; LAD = left anterior descending; SSF1 = SnapShot Freeze; SSF2 = SnapShot Freeze 2; STD = standard.

improve image quality, thereby enhancing the diagnostic accuracy of CT-FFR calculation.

The DeFACTO study showed that misalignment and motion-related artifacts limit the clinical application of CT-FFR [22]. Artifacts affect the accuracy of vessel segmentation, which is of utmost importance for precise blood flow simulations. Thus, postprocessing approaches aimed at artifact reduction have always attracted great interest. SSF1 holds substantial potential in overcoming the traditional limitations of CT imaging. Previous studies showed that SSF1 improves the image quality and evaluation of the coronary arteries in CCTA, which concurs with our study findings [23,24]. However, in our study, the application of SSF1 failed to significantly improve the accuracy of CT-FFR calculations, which may be attributed to the fact that SSF1 could not reduce motion artifacts for whole cardiac structures [25]. Similar to SSF1, SSF2 selects data from adjacent phases within the same cardiac cycle to track the movement path of the vessels and correct motion artifacts in individual phases [13]. Compared with SSF1, SSF2 not only further reduces motion artifacts in the coronary arteries of CCTA but also corrects motion artifacts related to the valves and myocardium, achieving an optimized freezing effect of the coronary artery images. In our study, SSF2 significantly improved the image quality scores of all three epicardial vessels, whereas SSF1 only enhanced the RCA score. Moreover, the diagnostic

Table 4
Diagnostic performance of CCTA and CT-FFR for identifying ischemic stenosis based on standard reconstruction and two motion correction algorithms.

Level	Measure	Group	Accuracy%	Sensitivity%	Specificity%	PPV%	NPV%
Per-lesion (n = 170)	LM DS ≥ 50 % or other epicardial vessels DS ≥ 70 %	STD	52.94 (90 / 170)	91.67 (77 / 84)	15.11 (13 / 86)	51.33 (77 / 150)	65.00 (13 / 20)
		SSF1	59.41 (101 / 170)	94.05 (79 / 84)	25.58 (22 / 86)	55.24 (79 / 143)	81.48 (22 / 27)
		P_1	0.077	0.157	0.067	0.327	<0.001
		SSF2	67.64 (115 / 170)	96.43 (81 / 84)	39.53 (34 / 86)	60.90 (81 / 133)	91.89 (34 / 37)
		P_2	0.002	0.359	<0.001	0.514	<0.001
		P_3	<0.001	0.359	0.005	0.448	<0.001
	CT-FFR ≤ 0.80	STD	72.94 (124 / 170)	82.14 (69 / 84)	63.95 (55 / 86)	69.00 (69 / 100)	78.57 (55 / 70)
		SSF1	78.24 (133 / 170)	84.52 (71 / 84)	72.09 (62 / 86)	74.74 (71 / 95)	82.67 (62 / 75)
		P_1	<0.001	0.157	0.106	0.230	0.073
		SSF2	86.47 (147 / 170)	90.48 (76 / 84)	82.56 (71 / 86)	83.51 (76 / 91)	89.87 (71 / 79)
		P_2	<0.001	0..071	0.018	0.134	0.009
		P_3	<0.001	0.198	0.067	0.259	0.049
Per-patient (n = 151)	LM DS ≥ 50 % or other epicardial vessels DS ≥ 70 %	STD	55.63 (84 / 151)	94.87 (74 / 78)	13.70 (10 / 73)	54.01 (74 / 137)	71.43 (10 / 14)
		SSF1	59.60 (90 / 151)	94.87 (74 / 78)	21.92 (16 / 73)	56.49 (74 / 131)	80.00 (16 / 20)
		P_1	0.042	0.339	0.101	0.494	<0.001
		SSF2	66.89 (101 / 151)	96.15 (75 / 78)	35.62 (26 / 73)	61.48 (75 / 122)	89.66 (26 / 29)
		P_2	0.002	0.558	0.001	0.669	<0.001
		P_3	<0.001	0.406	0.035	0.541	<0.001
	CT-FFR ≤ 0.80	STD	71.52 (108 / 151)	82.05 (64 / 78)	60.27 (44 / 73)	68.82 (64 / 93)	75.86 (44 / 58)
		SSF1	76.16 (115 / 151)	84.62 (66 / 78)	67.12 (49 / 73)	73.33 (66 / 90)	80.33 (49 / 61)
		P_1	<0.001	0.140	0.128	0.213	0.088
		SSF2	84.77 (128 / 151)	89.74 (70 / 78)	79.45 (58 / 73)	82.35 (70 / 85)	87.88 (58 / 66)
		P_2	<0.001	0.080	0.019	0.147	0.009
		P_3	<0.001	0.225	0.047	0.292	0.030

Abbreviations: CT-FFR = coronary computed tomography-derived fractional flow reserve; DS = diameter stenosis; LM = left main artery; NPV = negative predictive value; PPV = positive predictive value; SSF1 = SnapShot Freeze 1; SSF2 = SnapShot Freeze 2; STD = standard.
*Ischemic lesions was defined as stenosis with invasive FFR ≤ 0.8 or diameter stenosis of ≥ 90 %.
P_1:p-value for the comparison between the STD group and the SSF1 group.
P_2:p-value for the comparison between the STD group and the SSF2 group.
P_3:p-value for the comparison between the SSF1 group and the SSF2 group.

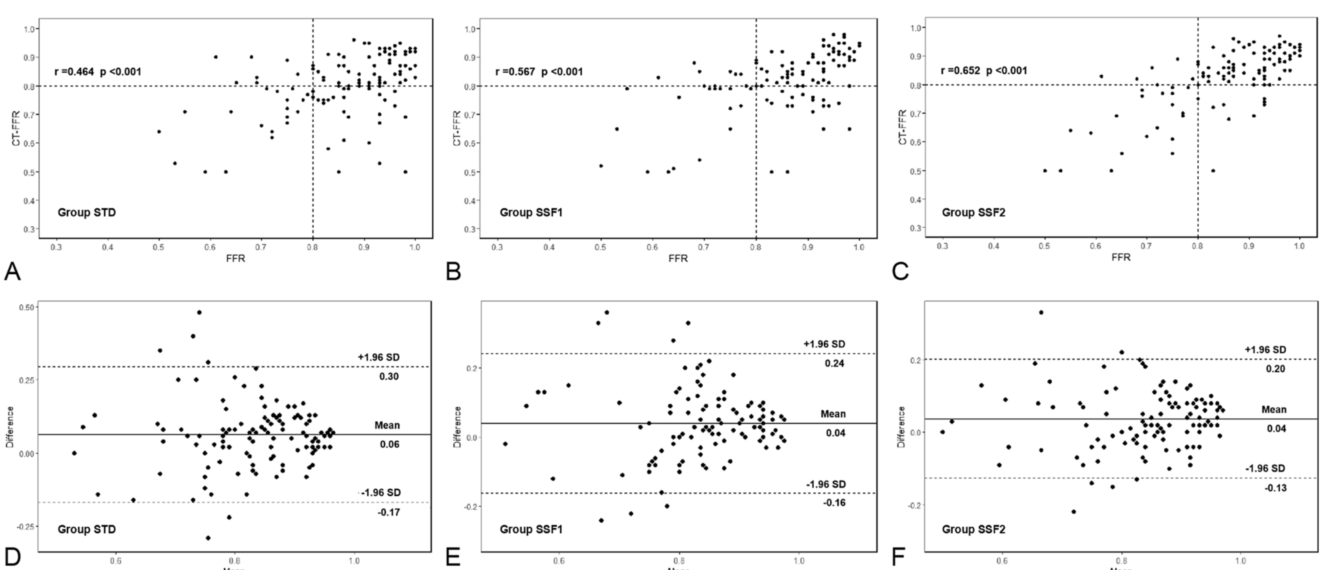

Fig. 4. Spearman's correlation coefficient (A-C) and Bland–Altman plot (D–F) between CT-FFR and FFR of the three groups. Abbreviations: CT-FFR = coronary computed tomography-derived fractional flow reserve; FFR = fractional flow reserve; SSF1 = SnapShot Freeze; SSF2 = SnapShot Freeze 2; STD = standard.

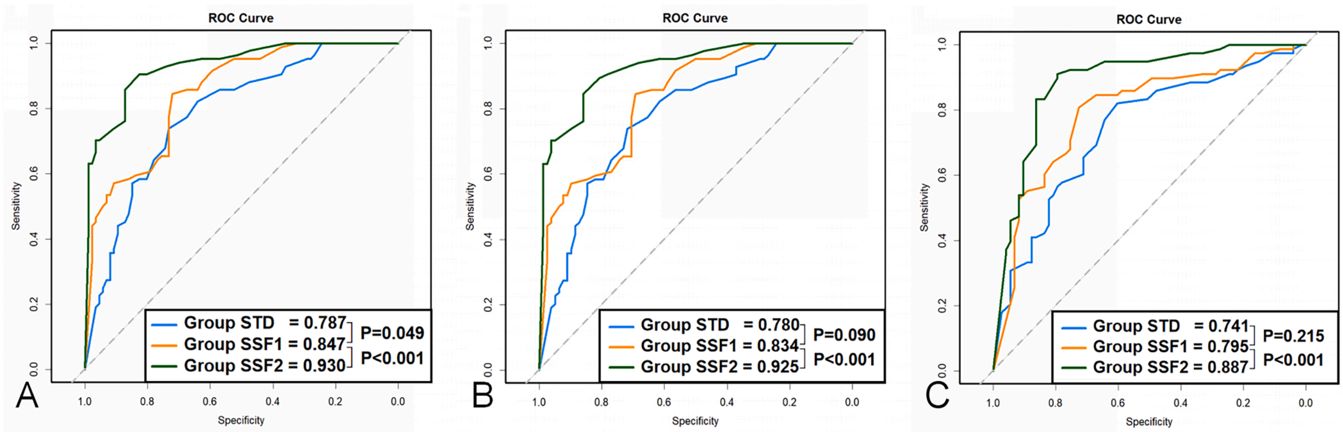

Fig. 5. ROC curves of the CT-FFR for the demonstration of ischemic stenosis at the per-lesion (A), per-vessel level (B) and per-patient level (C). Abbreviations: CT-FFR = coronary computed tomography-derived fractional flow reserve; FFR = fractional flow reserve; SSF1 = SnapShot Freeze; SSF2 = SnapShot Freeze 2; STD = standard.

accuracy of DS evaluated using CCTA and CT-FFR was also significantly enhanced because of the improved image quality. Because the coronary arteries traverse in the interventricular and atrioventricular grooves, they are prone to artifacts caused by the myocardial contraction movements of the adjacent atria and ventricles. The improvement of image quality with SSF2 may be attributed to further correction of the motion artifacts of myocardial movement. Thus, the application of SSF2 may have significant advantages in reducing motion artifacts, enhancing the image quality of CCTA, and consequently improving the diagnostic accuracy of CT-FFR.

The application of the SSF2 technique significantly enhanced the image quality and interpretability of CCTA, thereby improving the accuracy of CT-FFR evaluation. Compared with STD and SSF1, SSF2 significantly reduced the number of false-positive cases while maintaining a high NPV. Hence, it is conceivable that fewer patients would undergo unnecessary invasive procedures if the CT-FFR technique has a high PPV. This advancement supports the use of SSF2 in CT-FFR simulation as an increasingly reliable and effective tool for identifying hemodynamically significant stenoses, potentially aiding in guiding more precise treatment decisions and improving patient outcomes and safety.

This study has several limitations. Firstly, it was a single-center retrospective study with a relatively small sample size, particularly including fewer cases of high calcification burden (CACS $\geq$ 400). Further research is warranted to investigate the impact of calcification on CT-FFR. Secondly, in our study, it is notable that intermediate stenosis only account for a relatively small proportion of target lesions. It requires future prospective studies to validate the diagnostic performance of SSF2-based CT-FFR calculation in the specific group of borderline lesions. Finally, the application of the SSF2 algorithm was confined to vendor-specific CT data, limiting its broader implementation in diverse clinical settings.

In conclusion, the second-generation motion correction algorithm significantly improves CCTA image quality and, therefore, enhances the diagnostic performance of CT-FFR simulation.

Ethics approval

This retrospective study was reviewed and approved by *** Hospital Ethics Committee, and obtaining informed consent from all patients was exempted.

Funding

This study is supported by The National Key Research and Development Program of China (Grant No.: 2021YFF0501402), National Natural Science Foundation of China (Grant No.: 82271990), Shanghai Jiao Tong University "Star Project" of Biomedical Multi-discipline Research Program (Grant No.: YG2022ZD015), Shenkang 3-year project of clinical innovation (Grant No.: SHDC2022CRD016), and Shanghai Health Commission Discipline Leader Project (Grant No.: 2022XD031).

CRediT authorship contribution statement

Wenli Yang: Resources, Project administration. **Lihua Yu:** Software, Formal analysis. **Yarong Yu:** Investigation. **Xu Dai:** Visualization, Software. **Wenyi Yang:** Resources, Project administration. **Jiayin Zhang:** Writing – review & editing, Writing – original draft, Supervision, Project administration, Methodology, Funding acquisition, Conceptualization.

Declaration of competing interest

The authors declare that they have no known competing financial interests or personal relationships that could have appeared to influence the work reported in this paper.

Acknowledgement

We thank Mr. Shuai Zhang (from GE healthcare China) for his help in acquiring the access to Spapshot freezing 2 technique.

Appendix A. Supplementary data

Supplementary data to this article can be found online at https://doi.org/10.1016/j.ejrad.2024.111538.

References

[1] M. Gulati, P.D. Levy, D. Mukherjee, et al., 2021 AHA/ACC/ASE/CHEST/SAEM/SCCT/SCMR Guideline for the Evaluation and Diagnosis of Chest Pain: Executive Summary: A Report of the American College of Cardiology/American Heart Association Joint Committee on Clinical Practice Guidelines, Circulation 144 (2021) e368–e454, https://doi.org/10.1161/cir.0000000000001030.

[2] L.H. Nielsen, N. Ortner, B.L. Nørgaard, S. Achenbach, J. Leipsic, J. Abdulla, The diagnostic accuracy and outcomes after coronary computed tomography angiography vs. conventional functional testing in patients with stable angina pectoris: a systematic review and meta-analysis, Eur Heart J Cardiovasc Imaging 15 (2014) 961–971, https://doi.org/10.1093/ehjci/jeu027.

[3] K.M. Abdelrahman, M.Y. Chen, A.K. Dey, et al., Coronary Computed Tomography Angiography From Clinical Uses to Emerging Technologies: JACC State-of-the-Art Review, J Am Coll Cardiol 76 (2020) 1226–1243, https://doi.org/10.1016/j.jacc.2020.06.076.

[4] M.R. Patel, D. Dai, A.F. Hernandez, et al., Prevalence and predictors of nonobstructive coronary artery disease identified with coronary angiography in contemporary clinical practice, Am Heart J 167 (2014) 846–852.e842, https://doi.org/10.1016/j.ahj.2014.03.001.

[5] J. Knuuti, H. Ballo, L.E. Juarez-Orozco, et al., The performance of non-invasive tests to rule-in and rule-out significant coronary artery stenosis in patients with stable angina: a meta-analysis focused on post-test disease probability, Eur Heart J 39 (2018) 3322–3330, https://doi.org/10.1093/eurheartj/ehy267.

[6] B.L. Nørgaard, J. Leipsic, S. Gaur, et al., Diagnostic performance of noninvasive fractional flow reserve derived from coronary computed tomography angiography in suspected coronary artery disease: the NXT trial (analysis of coronary blood flow using CT angiography: next steps), J Am Coll Cardiol 63 (2014) 1145–1155, https://doi.org/10.1016/j.jacc.2013.11.043.

[7] H. Mickley, K.T. Veien, O. Gerke, et al., Diagnostic and Clinical Value of FFR(CT) in Stable Chest Pain Patients With Extensive Coronary Calcification: The FACC Study, JACC Cardiovasc Imaging 15 (2022) 1046–1058, https://doi.org/10.1016/j.jcmg.2021.12.010.

[8] S. Tu, J. Westra, J. Yang, et al., Diagnostic Accuracy of Fast Computational Approaches to Derive Fractional Flow Reserve From Diagnostic Coronary Angiography: The International Multicenter FAVOR Pilot Study, JACC Cardiovasc Interv 9 (2016) 2024–2035, https://doi.org/10.1016/j.jcin.2016.07.013.

[9] P. Rajiah, K.W. Cummings, E. Williamson, P.M. Young, CT Fractional Flow Reserve: A Practical Guide to Application, Interpretation, and Problem Solving, Radiographics 42 (2022) 340–358, https://doi.org/10.1148/rg.210097.

[10] J. Leipsic, T.M. Labounty, C.J. Hague, et al., Effect of a novel vendor-specific motion-correction algorithm on image quality and diagnostic accuracy in persons undergoing coronary CT angiography without rate-control medications, J Cardiovasc Comput Tomogr 6 (2012) 164–171, https://doi.org/10.1016/j.jcct.2012.04.004.

[11] J. Liang, H. Wang, L. Xu, et al., Impact of SSF on diagnostic performance of coronary computed tomography angiography within 1 heart beat in patients with high heart rate using a 256-row detector computed tomography, J Comput Assist Tomogr 42 (2018) 54–61, https://doi.org/10.1097/rct.0000000000000641.

[12] J. Liang, H. Wang, L. Xu, et al., Diagnostic performance of 256-row detector coronary CT angiography in patients with high heart rates within a single cardiac cycle: a preliminary study, 694.e697–694.e614, Clin Radiol 72 (2017), https://doi.org/10.1016/j.crad.2017.03.004.

[13] Y. Matsumoto, C. Fujioka, K. Yokomachi, et al., Evaluation of the second-generation whole-heart motion correction algorithm (SSF2) used to demonstrate the aortic annulus on cardiac CT, Sci Rep 13 (2023) 3636, https://doi.org/10.1038/s41598-023-30786-7.

[14] M.Y. Chen, S.M. Shanbhag, A.E. Arai, Submillisievert median radiation dose for coronary angiography with a second-generation 320-detector row CT scanner in 107 consecutive patients, Radiology 267 (2013) 76–85, https://doi.org/10.1148/radiol.13122621.

[15] Z. Li, G. Li, L. Chen, et al., Comparison of coronary CT angiography-based and invasive coronary angiography-based quantitative flow ratio for functional assessment of coronary stenosis: A multicenter retrospective analysis, J Cardiovasc Comput Tomogr 16 (2022) 509–516, https://doi.org/10.1016/j.jcct.2022.06.002.

[16] Z. Li, J. Zhang, L. Xu, et al., Diagnostic Accuracy of a Fast Computational Approach to Derive Fractional Flow Reserve From Coronary CT Angiography, JACC Cardiovasc Imaging 13 (2020) 172–175, https://doi.org/10.1016/j.jcmg.2019.08.003.

[17] Y.O. Nozaki, S. Fujimoto, Y.O. Kawaguchi, et al., Prognostic value of the optimal measurement location of on-site CT-derived fractional flow reserve, J Cardiol 80 (2022) 14–21, https://doi.org/10.1016/j.jjcc.2022.02.019.

[18] J. Westra, Z. Li, L.D. Rasmussen, et al., One-step anatomic and function testing by cardiac CT versus second-line functional testing in symptomatic patients with coronary artery stenosis: head-to-head comparison of CT-derived fractional flow reserve and myocardial perfusion imaging, EuroIntervention 17 (2021) 576–583, https://doi.org/10.4244/eij-d-20-00905.

[19] Y. Li, M. Yu, X. Dai, et al., Detection of hemodynamically significant coronary stenosis: CT myocardial perfusion versus machine learning CT fractional flow reserve, Radiology 293 (2019) 305–314, https://doi.org/10.1148/radiol.2019190098.

[20] P.S. Douglas, B. De Bruyne, G. Pontone, et al., 1-Year Outcomes of FFRCT-Guided Care in Patients With Suspected Coronary Disease: The PLATFORM Study, J Am Coll Cardiol 68 (2016) 435–445, https://doi.org/10.1016/j.jacc.2016.05.057.

[21] P.P. Xu, J.H. Li, F. Zhou, et al., The influence of image quality on diagnostic performance of a machine learning-based fractional flow reserve derived from coronary CT angiography, Eur Radiol 30 (2020) 2525–2534, https://doi.org/10.1007/s00330-019-06571-4.

[22] J. Leipsic, T.H. Yang, A. Thompson, et al., CT angiography (CTA) and diagnostic performance of noninvasive fractional flow reserve: results from the Determination of Fractional Flow Reserve by Anatomic CTA (DeFACTO) study, AJR Am J Roentgenol 202 (2014) 989–994, https://doi.org/10.2214/ajr.13.11441.

[23] H.M. Sheta, K. Egstrup, M. Husic, L.J. Heinsen, K. Nieman, J. Lambrechtsen, Impact of a motion correction algorithm on image quality in patients undergoing CT angiography: A randomized controlled trial, Clin Imaging 42 (2017) 1–6, https://doi.org/10.1016/j.clinimag.2016.11.002.

[24] H.M. Sheta, K. Egstrup, M. Husic, L.J. Heinsen, J. Lambrechtsen, Impact of a motion correction algorithm on quality and diagnostic utility in unselected patients undergoing coronary CT angiography, Clin Imaging 40 (2016) 217–221, https://doi.org/10.1016/j.clinimag.2015.10.007.

[25] H. Machida, R. Fukui, J. Gao, et al., Reduction of Coronary Motion Artifacts in Prospectively Electrocardiography-Gated Coronary Computed Tomography Angiography Using Monochromatic Imaging at Various Energy Levels in Combination With a Motion Correction Algorithm on Single-Source Fast Tube Voltage Switching Dual-Energy Computed Tomography: A Phantom Experiment, Invest Radiol 51 (2016) 513–519, https://doi.org/10.1097/rli.0000000000000263.